PAPER • OPEN ACCESS

Structural and magnetic studies of the frustrated $S = 1$ kagome magnet $NH_4Ni_2Mo_2O_{10}H_3$

View the article online for updates and enhancements.

Structural and magnetic studies of the frustrated $S = 1$ kagome magnet NH$_4$Ni$_2$Mo$_2$O$_{10}$H$_3$

E T Connolly[1,2,*] , **J Wardell**[1], **D Boldrin**[2] , **C C Tang**[2] and **A S Wills**[1]

[1] Department of Chemistry, UCL, 20 Gordon St, London WC1H 0AJ, United Kingdom
[2] Diamond Light Source, Harwell Science and Innovation Campus, Didcot OX11 0DE, United Kingdom
[3] School of Physics & Astronomy, Kelvin Building, University of Glasgow, Glasgow G12 8QQ, United Kingdom

E-mail: eamonn.connolly@diamond.ac.uk

CrossMark

Abstract

The strong geometric frustration of the kagome antiferromagnets (KAFMs) can destabilise conventional magnetic order and lead to exotic electronic states, such as the quantum spin-liquid state observed in some $S = \frac{1}{2}$ KAFM materials. However, the ground state of $S = 1$ KAFM systems are less well understood. Spin nematic phases and valence bond solid ground states have been predicted to form but a paucity of experimental realisations restricts understanding. Here, the $S = 1$ KAFM NH$_4$Ni$_2$Mo$_2$O$_{10}$H$_3$ is presented, which has the 3-fold symmetry of the kagome lattice but significant site depletion, with ~64% site occupancy. Frustration and a competition between exchange interactions are evidenced through the suppression of order below the Weiss temperature $|\theta_W|$ and observation of ferromagnetic and antiferromagnetic characteristics in the magnetisation data. A semi spin glass ground state is predicted based on the ac-field frequency dependence of the magnetic transition and ferromagnetic signal.

Supplementary material for this article is available online

1. Introduction

The strong geometric frustration of kagome antiferromagnets (KAFMs) is well known to destabilise conventional Néel order and drive the formation of exotic ground states, such as the topologically ordered quantum spin-liquid (QSL) ground state characterised by quasi-particle spinon excitations and predicted to underpin the high-T_C superconductor state [1–11].

Destabilised Néel order is maximal in $S = \frac{1}{2}$ KAFMs where large quantum fluctuations between the degenerate energy states combine with the strong geometric frustration, and as such QSL states have been observed in the $S = \frac{1}{2}$ KAFM paratacamite minerals, hebertsmithite (γ-ZnCu$_3$(OH)$_6$Cl$_2$) [12, 13] and its polymorph kapellasite (α-ZnCu$_3$(OH)$_6$Cl$_2$) [14, 15]. Away from the well studied $S = \frac{1}{2}$ KAFMs, the ground states of the semi-classical $S = 1$ kagome magnets are relatively little understood. It is uncertain whether the reduced strength of quantum fluctuations in the $S = 1$ systems, compared to $S = \frac{1}{2}$ equivalents, is strong enough to destabilise conventional magnetic order, and the role played by the integer physics is much debated. For example, the $S = 1$ kagome Heisenberg antiferromagnet modelled using the coupled cluster approach displayed an absence of magnetic

order due to quantum fluctuations [16, 17], whilst a quantum many-body Heisenberg model suggests that magnetic order is induced by the integer nature of the spin [18]. The ordered ground state of the $S = 1$ kagome Heisenberg antiferromagnet based on nearest-neighbour and further-neighbour exchange is believed to be a type of valence bond solid, such as the triangular valence bond solid (TVBS) [19–22] or hexagonal singlet solid (HSS) [23], which consist of entangled spin singlets arranged around the respective triangles and hexagons of the kagome lattice. Furthermore, spin nematic phases are predicted to form when small energy terms important for $S = 1$ systems are included in the magnetic Hamiltonian, such as single-ion anisotropy and biquadratic exchange [24, 25].

The library of $S = 1$ KAFM magnetic materials available to explore such ground states is relatively small, especially in comparison to known quantum and classical materials, and those studied show a diverse range of magnetic behaviour. The $S = 1$ KAFM materials, NaV_6O_{11} and *m*-MPYNN·BF$_4$, evidence spin gapped non-magnetic ground states which are candidate valence bond solids [26, 27]. The $S = 1$ kagome antiferromagnetic lattice of *m*-MPYNN·BF$_4$ only forms at $T < 20$ K, when the $S = \frac{1}{2}$ MPYNN (*m*-N-methylpyridium α-nitronyl nitroxide) organic-radicals dimerise *via* ferromagnetic exchange [26, 28]. For NaV_6O_{11}, the magnetic response is a combination of the $S = 1$ V^{3+} ions, which make up the kagome lattice, and $S = \frac{1}{2}$ V^{4+} ions, which lie between the kagome planes [27, 29]. Another significant $S = 1$ KAFM is $KV_3Ge_2O_9$, which has an ideal 2-dimensional kagome lattice of $S = 1$ V^{3+} ions. Magnetometry performed on single crystal samples reveals short-range magnetic order at $T_p \lesssim 70$ K and the bifurcation between in- and out-of-plane susceptibility at $T \lesssim 25$ K [30], which rules out the possibility of a singlet ground state. Other $S = 1$ kagome materials—such as $AV_3(SO_4)_2(OH)_6$ ($A = Na^+$, K^+) [31], $BaNi_3V_2O_8(OH)_2$ [32, 33] and $YCa_3(VO)_3(BO_3)_4$ [34]—display a range of unconventional ground states, which include QSL and spin glass states in $YCa_3(VO)_3(BO_3)_4$ and $BaNi_3V_2O_8(OH)_2$ respectively, which exist despite an absence of intra-kagome geometric frustration. The $S = 1$ KAFM materials $[C_6N_2H_8][NH_4]_2[Ni_3F_6(SO_4)_2]$ [35], $(NH_4)_2(C_2H_8N)[V_3F_{12}]$ [36] and $NH_4Ni_{2.5}V_2O_7(OH)_2·H_2O$ [37] display magnetic frustration which results from 2-dimensional kagome lattices and dominant antiferromagnetic exchange interactions. Alongside this each of these materials display a small ferromagnetic competent, a response assigned to either canted antiferromagnetic spin structures or competing types of exchange. The wide range of experimental responses displayed by the limited library of known $S = 1$ KAFM materials, promotes considerable interest in the discovery of further experimental systems such as the $S = 1$ kagome magnet $NH_4Ni_2Mo_2O_{10}H_3$ characterised in this work.

In this manuscript, we show $NH_4Ni_2Mo_2O_{10}H_3$ has ideal kagome geometry in which to explore frustrated physics, with a highly 2-dimensional isotropic kagome lattice of $S = 1$ Ni^{2+} ions, the structure of which was previously reported [38–40]. Structural analysis of the $\angle Ni$–O–Ni bond angles suggests there is a competition between nearest-neighbour

antiferro- and ferromagnetic superexchange. Our magnetisation data show a suppression of magnetic order ($T_C \approx 13.5$ K) below the Weiss temperature ($\theta_W \sim -73$ K) and a corresponding build-up of antiferromagnetic short-range spin correlations, evidenced by deviations from the Curie–Weiss law, common signatures of magnetic frustration. Moreover, frequency-dependent changes to the magnetic transition in ac-susceptibility $\chi'(T)$ data suggest spin glasslike properties. Low-temperature field-dependant magnetisation studies reveal coercive behaviour in a weak ferromagnetic response similar to $[C_6N_2H_8][NH_4]_2[Ni_3F_6(SO_4)_2]$, $(NH_4)_2(C_2H_8N)[V_3F_{12}]$ and $NH_4Ni_{2.5}V_2O_7(OH)_2·H_2O$.

2. Experimental

The synthesis of $NH_4Ni_2Mo_2O_{10}H_3$ was adapted from a previously presented series [38, 41, 42]. $Ni(NO_3)_2·6$ H_2O (1.1632 g, $\geqslant 98$ %, Fisher) and $(NH_4)_6Mo_7O_{24}4·4$ H_2O (0.7062 g, 99.98%, Sigma-Aldrich) were added to 100 ml volume single-neck round bottom flask and dissolved in 30 ml of distilled water to give a solution of pH = 4.60. The round bottom flask with an attached condenser tube was heated to $T = 90 °C$ and concentrated NH_4OH (28% wt, Sigma-Aldrich) was then added drop-wise with continual stirring to give a deep blue solution of pH = 10.0. The solution was heated at $T = 90$ °C for 8 h during which a green precipitate of $NH_4Ni_2Mo_2O_{10}H_3$ formed. The product was vacuum filtered and rinsed with water until the solution ran clear and then dried in an oven at $T = 100$ °C for 12 h. The final product was a green powder with a mass of 527 mg.

A room temperature synchrotron x-ray powder diffraction (SXPD) pattern of $NH_4Ni_2Mo_2O_{10}H_3$ was collected at the I11 beamline of the Diamond Light Source, UK, where the high-resolution MAC detector array was utilised. The SXPD pattern was collected using a wavelength of $\lambda = 0.826\,566(10)$ Å with the sample held in a spinning 0.3 mm diameter borosilicate glass capillary. The wavelength was calibrated using the pattern of a high-quality Si standard and chosen to help maximise the flux of incident radiation whilst minimising absorption by the heavy Mo^{6+} ions. Assuming a packing fraction of 0.6, absorption was calculated as $\mu R \approx 0.9$, which is close to the ideal value of 1 for x-ray powder diffraction. Bulk magnetometry data were collected using a Quantum Design MPMS-3 on a sample packed into a gelatin capsule and corrected for the diamagnetic contribution of the refined structural formula using literature Pascal's constants [43].

3. Crystal structure analysis

The initial structural model used in the refinement of $NH_4Ni_2Mo_2O_{10}H_3$ was taken from *Levin et al* [38], and a total of 62 parameters were refined (table S1). Figure 1 shows the good agreement between the experimental and calculated data as indicated by $R_{wp} = 8.105$ and $\chi^2 = 1.331$. The crystal structure information obtained from the refinement is summarised in table 1. $NH_4Ni_2Mo_2O_{10}H_3$ has a layered structure of NiO_6 octahedral edge-sharing sheets stacked along the
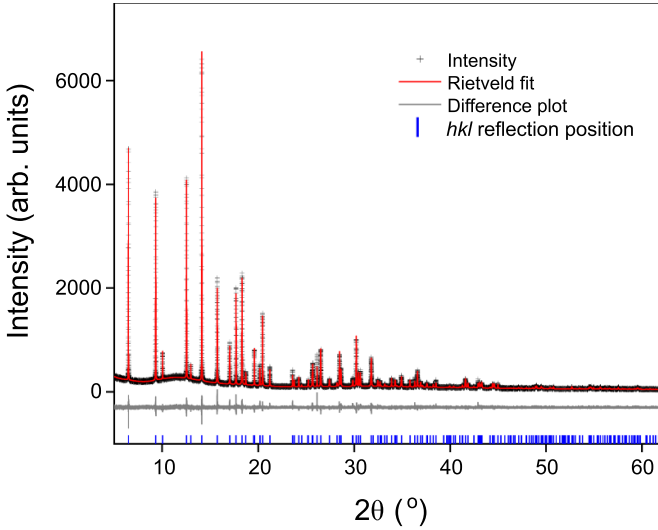
Figure 1. Experimental SXPD pattern of $NH_4Ni_2Mo_2O_{10}H_3$ ($\lambda = 0.826566$ Å) recorded on the I11 beamline of the Diamond Light Source. Shown are the calculated Rietveld fit to the data, difference plot and reflection positions, which are represented by the vertical tick marks. The goodness-of-fit is $\chi^2 = 1.331$ and weighted R-value is $R_{wp} = 8.105$, with 62 variables refined.

randomness-induced QSLs [46], of which $S = \frac{1}{2}$ kagome anti-ferromagnetic Zn-brochantite ($ZnCu_3(OH)_6SO_4$) is a candidate system [47, 48].

Two superexchange pathways are present in $NH_4Ni_2Mo_2O_{10}H_3$, mediated by the O(H) and O(3) oxygens, where Ni–O(H)–Ni $= 98.66(12)°$ and Ni–O(3)–Ni $= 85.71(8)°$. These bond angles are expected to correspond to antiferro- and ferro-magnetic exchange pathways, respectively, following the Goodenough–Kanamori–Anderson rules [49, 50]: where bond angles >90 ° facilitate anti-parallel (antiferromagnetic) spin alignment. Further to this, various magnetometry studies of Ni(II) oxide complexes show the cross over angle from ferromagnetic to antiferromagnetic superexchange is Ni $-$ O $-$ Ni $> 96 - 99$ ° [51–53]. It follows that a competition between the nearest-neighbour antiferro- and ferromagnetic exchange is expected and that this would cause a reduced overall strength of the exchange field. At the same time, such a competing exchange may also create or support degeneracies in the ground state. An example of this situation is found in kapellasite, where competing nearest-neighbour ferromagnetic exchange and further neighbour anti-ferromagnetic exchange produce a chiral spin-liquid ground state [15].

4. Magnetic characterisation

Zero-field cooled (ZFC) and field cooled (FC) data were collected from $NH_4Ni_2Mo_2O_{10}H_3$ in a field of 500 Oe between 2 and 300 K. Figure 3(a) shows the temperature-dependence of the inverse susceptibility. A fit to the high-temperature linear region of the graph over the range 225–300 K and extrapolation following the Curie–Weiss law allows the Weiss temperature to be estimated as $\theta_W \sim -73$ K, indicating a net antiferromagnetic mean field. Deviation from the linear Curie-Weiss regime below $T \sim 220$ K, approximately $3\theta_W$, evidences a build-up of short-range super-paramagnetic spin correlations significantly above the transition temperature—a behaviour commonly observed in frustrated magnets [14, 55, 56]. The low temperature region of the susceptibility data (figure 3(b)) shows an increase in susceptibility characteristic of a magnetic transition below $T \sim 24$ K with a maximum in the gradient at $T_C \simeq 13.5$ K. The bifurcation of the ZFC and FC susceptibility data below $T \sim 10$ K is compatible with a small ferromagnetic contribution to the magnetic order, in contrast to the antiferromagnetic character of the mean field. The Landé g-factor value of 2.04, calculated from the room temperature effective moment of $\mu_{eff} = 2.88$ μ_B Ni^{-1}, is close to the expected spin-only value.

Alternating current (ac) susceptibility measurements of $NH_4Ni_2Mo_2O_{10}H_3$ were collected for varying ac frequencies between 2–20 K with $H_{ac} = 2$ Oe and a direct current (dc) field $H_{dc} = 0$ Oe (figure 4(a)). The peak in $\chi'(T)$ at $T < 20$ K results from the magnetic transition, the maximum of which shifts to lower temperature at decreasing frequency. The peak maximum represents the freezing temperature (T_f) for a spin glass, and a shift in the maximum of $\Delta T_f = 0.25$ is observed

c-axis and separated by MoO_4 tetrahedra and an interstitial NH_4^+ unit (figure 2(a)). In the stoichiometric compound, Ni^{2+} ($S = 1$) ions decorate $\frac{2}{3}$ of the 9e Wyckoff site which forms the $S = 1$ magnetic kagome lattice which allows for geometric frustration. Our refinements have good agreement with this structure and indicate that ~ 64 % of the kagome sites are occupied.

A high degree of magnetic 2-dimensionality is expected within this material as neighbouring kagome planes are separated by the MoO_4 tetrahedra, with ~ 5.48 Å spacing between layers and the absence of any obvious interlayer exchange pathways. Initial refinements produced a large thermal parameter for the O(2), in agreement with the previously refined value of $B_{iso} = 7.6$ Å^2[38]. The O(2) site lies at the vertex of the MoO_4 tetrahedra, with the Mo—O(2) bond pointing along the *c*-axis towards the μ_3—O(H) site on the adjacent kagome layer. Refinements where the O(2) was taken from the 6c Wyckoff site and moved away from the 3-fold rotational axis gave a more physically reasonable model of the disordered O(2) site, table 1.

$NH_4Ni_2Mo_2O_{10}H_3$ displays significant magnetic lattice site depletion with 64 % Ni-site occupancy. This occupancy is close to the site percolation threshold ($p_c^{site} = 65$ %) for nearest-neighbour interactions on a kagome lattice [44], below which we would expect the quenched disorder of a spin glass state. Henley showed the situation is more complex for significant non-magnetic impurities on a classical kagome lattice where the ordered ground state is robust to impurities [45], and for the diluted $S = 1$ kagome system a valence bond solid ground state with $S = \frac{1}{2}$ defect moments was predicted. Moreover, randomness such as defects may couple with quantum fluctuations and geometric frustration to form

Table 1. Fractional atomic coordinates, site occupancy and isotropic thermal parameters of $NH_4Ni_2Mo_2O_{10}H_3$ ($R\bar{3}m$, $a = 6.0382(2)$ Å, $c = 21.9320(7)$ Å). The final weighted R-value for the data is $R_{wp} = 8.105$ and the goodness-of-fit is $\chi^2 = 1.331$.

Name	Wyckoff site	x	y	z	B_{iso} (Å^2)	Occ.
Mo	$6c$	0	0	0.087 88(3)	2.582(18)	1
Ni	$9e$	0.5	0	0	1.34(3)	0.6379(16)
O(H)	$6c$	0	0	0.289 53(16)	3.70(11)	1
O(2)	$18h$	0.9615(6)	0.0385(13)	0.164 79(18)	1.58(16)	$\frac{1}{3}$
O(3)	$18h$	0.3212(5)	0.1606(2)	$-0.060\,72(8)$	3.59(6)	1
N	$3b$	0	0	0.5	1.43(12)	1

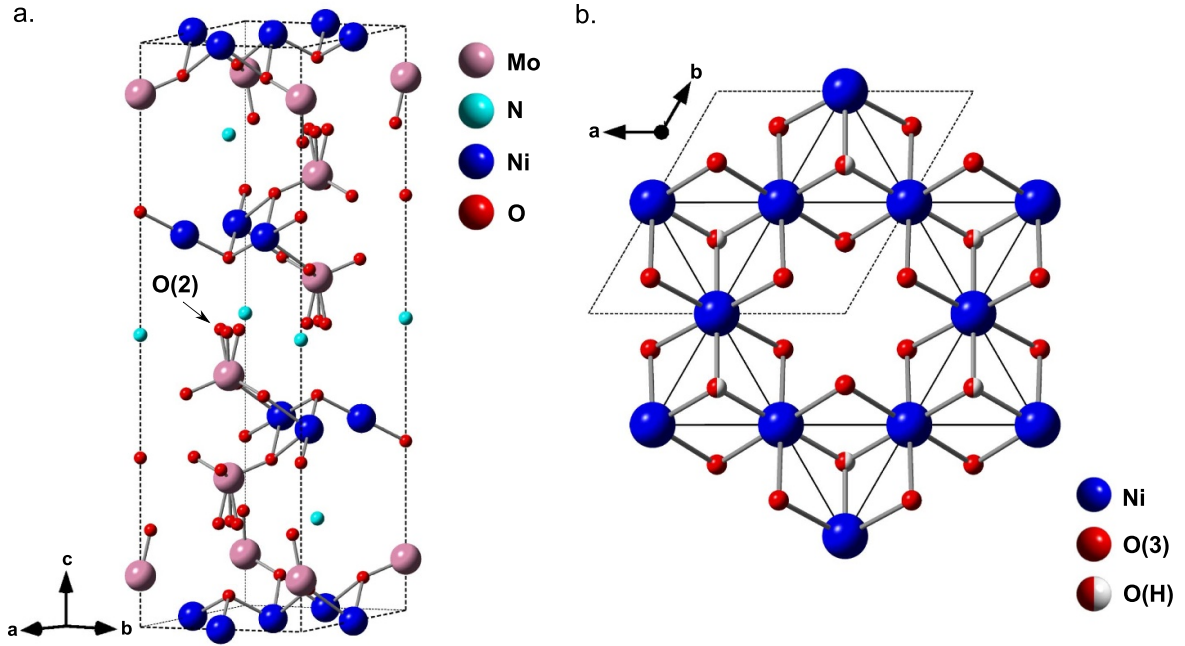**Figure 2.** (a) The structure of $NH_4Ni_2Mo_2O_{10}H_3$ in a single unit cell. Layers of edge-sharing NiO_6 octahedra are separated by MoO_4 tetrahedra and interstitial ammonium ions. The disordered O(2) site is labelled (b) The kagome lattice viewed along the c-axis. The Ni^{2+} ions occupy the vertex of the equilateral triangles that make up the kagome lattice. The O(H) and O(3) sites are expected to mediate antiferromagnetic and ferromagnetic exchange, respectively. The unit cell and kagome lattice are represented by the respective dashed and bold black lines.

for a $\Delta\nu = 299$ Hz frequency change. A Mydosh parameter ($K = \frac{\Delta T_f}{T_f\, log(\Delta\nu)}$) of 0.008 temperature shift per decade is calculated for $T_f = 12.5$ K: extracted from the $\nu = 1$ Hz $\chi'(T)$ plot [57]. This value is less than the 0.1 expected for a spin glass state and differentiates this magnetic response from one generated by superparamagnetic correlations ($K = 0.1 - 0.28$) [58]. Figure 4(b) shows further ac measurements as a function of dc-field from 2–40 K, with an ac-field frequency of $\nu = 100$ Hz: an ac-field of $H_{ac} = 1$ Oe was applied for all dc-fields except for $H_{dc} = 0$ Oe, where the ac-field was $H_{ac} = 2$ Oe. The imaginary $\chi''(T)$ component of the susceptibility shows the build up of a sharp cusp in $\chi''(T)$ with decreasing H_{dc} strength. At $H_{dc} = 0$ Oe a split peak is observed with maximums at $T_1 = 9.02$ K and $T_2 = 12.05$ K. These split peaks in ac susceptibility as a function of dc-fields are associated with co-existing states such as the 'semi spin glass' state. A similar response was observed in Co_2SnO_4, which hosts ferrimagnetic longitudinal order and a transverse spin-glass state [59].

$M(H)$ data were collected at 2 and 40 K to explore the magnetic response either side of the transition. Figure 5(a) shows a field-dependent hysteresis at $T = 2$ K that confirms a long-ranged ferromagnetic contribution to the magnetic transition. No saturation of the magnetic field is observed up to 7 T. An adapted magnetisation function was fitted to the data collected at 2 K between 2 and 7 T (figure 5(a)) to extract an estimate of the ferromagnetic contribution to the total signal [37]:

$$M(H) = M_{sat}\left[(1-f)B_J(H) + f\right]. \tag{1}$$

Here, f represents the proportion of ferromagnetic response to the total signal, $M_{sat} = gJN\mu_B$. B_J describes an effective field that is Brillouin-like and can be characterised as an adapted-Brillouin function per mole,

$$B_J(H) = \frac{2J+1}{2J}\coth\left(\frac{2J+1}{2J}y\right) - \frac{1}{2J}\coth\frac{y}{2J} \tag{2}$$
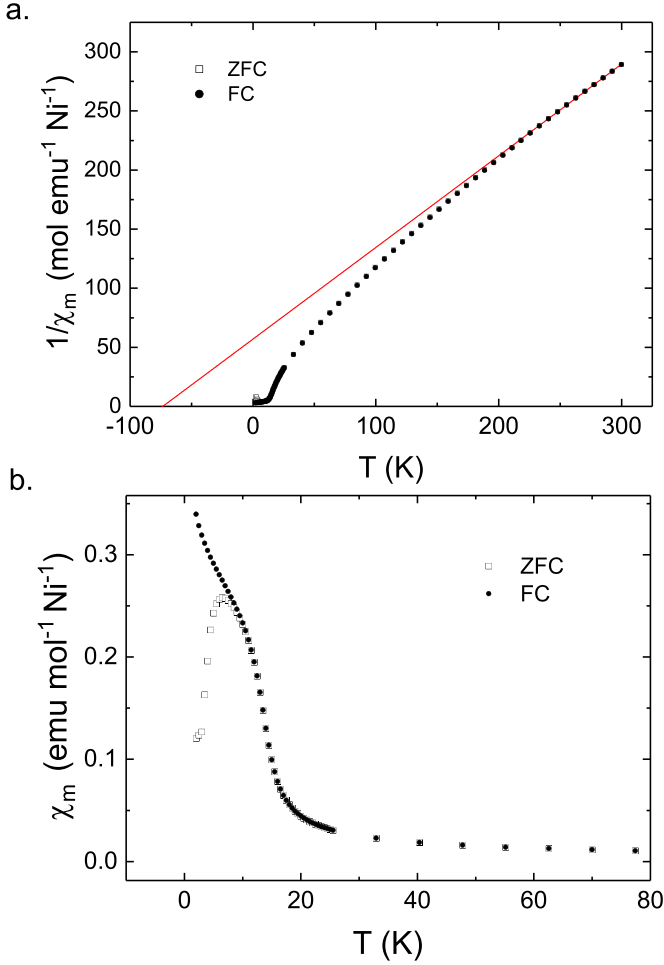
Figure 3. (a) Plot of the FC and ZFC inverse susceptibility *vs T* with a Curie–Weiss plot that indicates a Weiss temperature of $\theta_W \approx -73$ K and the build up of short range spin correlations at $T \approx 220$ K (b) Low temperature region of the $\chi(T)$ plot where magnetic order is observed at $T_C = 13.5$ K. Bifurcation between ZFC and FC at $T \approx 10$ K is observed due to a ferromagnetic component to the magnetic order [54].

Figure 4. (a) Plot of ac $\chi'(T)$ for ac-field frequencies from $\nu = 1 - 300$ Hz with an ac-field of $H_{ac} = 2$ Oe and a dc-field of $H_{dc} = 0$ Oe. A shift in the maximum (T_f) is shown to lower temperature with decreasing frequency (b) $\chi''(T)$ as a function of dc-field at $\nu = 100$ Hz: for $H_{dc} = 0$ Hz the ac-field is $H_{ac} = 2$ Oe, at all other dc-fields $H_{ac} = 1$ Oe. For $H_{dc} = 0$ Hz, the peak in $\chi''(T)$ has two maximums and could represent 2 separate transitions **Inset:** Sharp cusp in $\chi'(T)$ transition as dc-field decreases, a response characteristic of a spin glass state.

where $y = g\mu_B J H / k_B T_{eff}$ and $T_{eff} = T + T_0$. T_0 is a phenomenological parameter which accounts for the interactions between Ni^{2+} spins and is expected to be positive for antiferromagnetic interactions [60]. Table 2 displays the refined values of M_{sat}, f, and T_0 extracted from magnetisation data between $2 - 7$ T using the adapted magnetisation function.

Figure 5(b) shows a plot of the ferromagnetic contribution to the magnetisation at 2 K, isolated from recorded $M(H)$ data through the removal of the Brillouin-like contribution, from which a spontaneous moment of 0.026 μ_B Ni^{-1} and coercive field of 0.1 T can be determined. The plot shows the ferromagnetic component saturates at ~ 0.10 μ_B Ni^{-1}, which represents $\sim 5\%$ of the 2.04 μ_B Ni^{-1} signal expected if the Ni^{2+} spins were fully ordered.

Additional field-dependent magnetisation data were collected at 7.5, 13 and 25 K to determine the temperature-dependence of the Brillouin-like response over the temperature range where magnetic order is observed, and the fits to all the magnetisation data are shown in figure 5(c). The
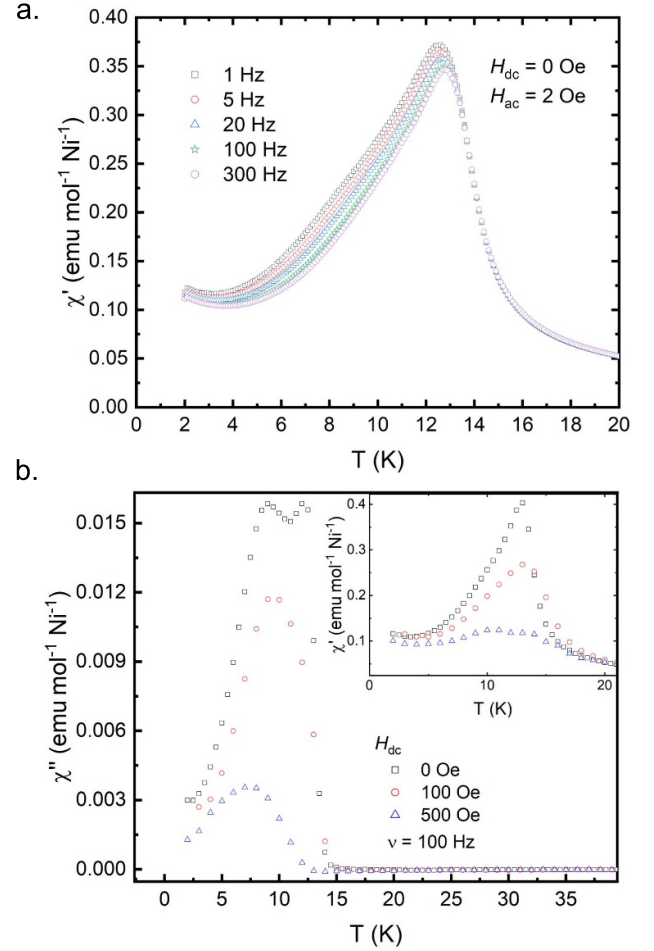
data at $T = 40$ K, is above the magnetic transition and was fitted using a standard magnetisation function, which yielded a saturated magnetisation of $M_{sat} = 1.367(1)$ μ_B Ni^{-1}, which is lower than the expected value of 2.04 μ_B Ni^{-1}. This is a result of the short-ranged ordering of the superparamagnetic region, with such reductions observed in the frustrated kagome magnets barlowite [61], herbertsmithite [62], and $NH_4Ni_{2.5}V_2O_7(OH)_2 \cdot H_2O$ [37].

Figure 5(d) shows plots of the refined f, M_{sat}, and T_0 parameters against temperature for the data collected at $T \leqslant 25$ K. These refined values are shown in table 2. The change in sign of the refined temperature parameter, T_0, on cooling below the transition, suggests the interactions between spins that form the Brillouin-like interaction field change from being net ferromagnetic to antiferromagnetic. The increase on cooling in the value of the ferromagnetic proportion, f, simultaneously with the increase in the antiferromagnetic behaviour characterised
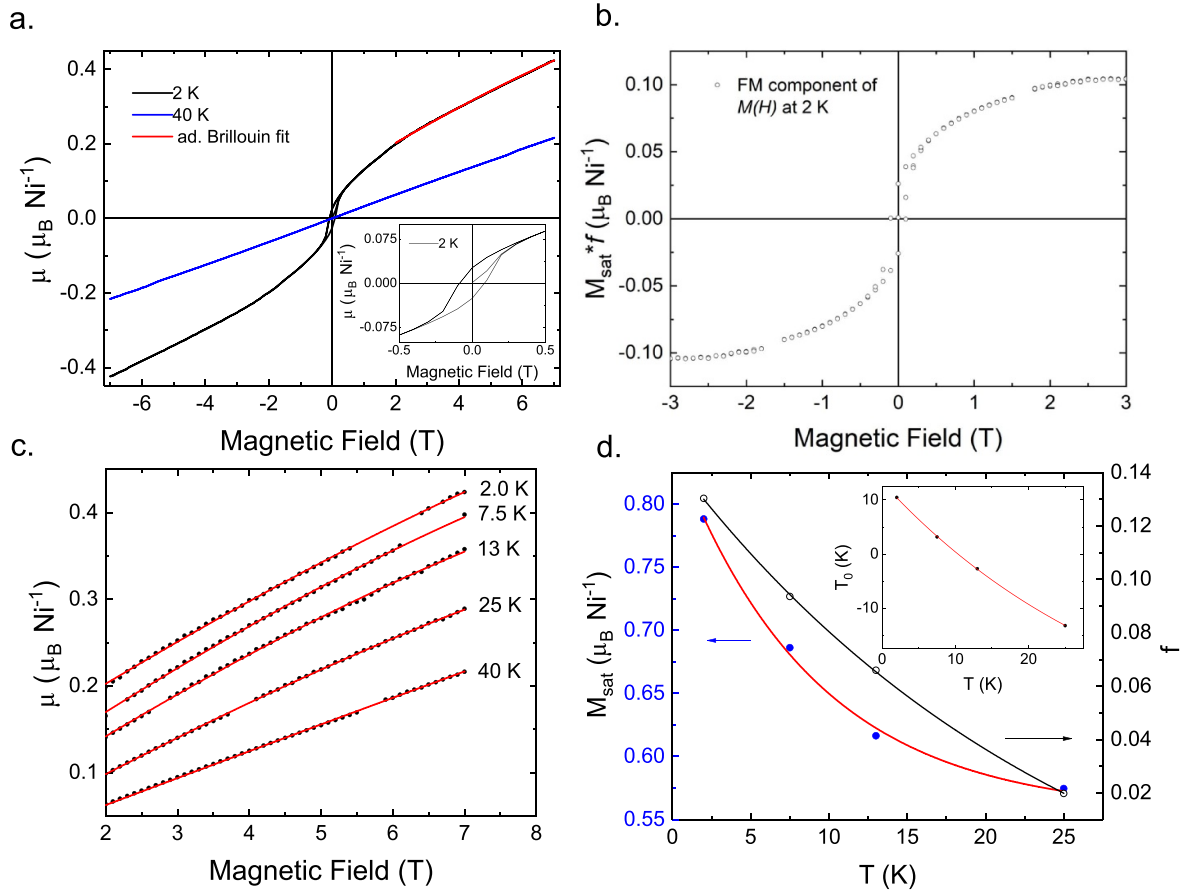
Figure 5. (a) $M(H)$ data recorded on $NH_4Ni_2Mo_2O_{10}H_3$ between -7 and 7 T that shows the hysteresis at $T = 2$ K. $M(H)$ data recorded above the transition at $T = 40$ K displays an absence of hysteresis. An adapted Brillouin function was fitted to the data at $T = 2$ K between 2 and 7 T **Inset:** Magnified plot of $M(H)$ data recorded at 2 K (b) A plot of the ferromagnetic component, $M_{sat} * f$, extracted from the 2 K $M(H)$ data using the adapted-Brillouin function, where a small spontaneous moment of 0.026 μ_B Ni^{-1} and coercive field of 0.1 T are observed (c) The adapted Brillouin function was fitted to $M(H)$ plots between 2 to 7 T for data collected at 2, 7.5, 13, 25, and 40 K with the refined parameters displayed in table 2 (d) Plots of M_{sat} and the ferromagnetic proportion, f, as a function of temperature show the build up of magnetic order at $T < 25$ K **Inset:** The plot of T_0 against temperature indicates the build up of antiferromagnetic correlations at low temperatures [54].

Table 2. Refined T_0, f, and M_{sat} values from the adapted magnetisation function fitted to the $M(H)$ plots collected at $T \leqslant 25$ K. The $M(H)$ data collected at $T = 40$ K was fitted with a standard magnetisation function with a refined M_{sat} value [54].

T (K)	T_0 (K)	f	M_{sat} (μ_B Ni^{-1})
40	—	—	1.367(1)
25	$-13.2(3)$	0.020(1)	0.57(1)
13	$-2.7(3)$	0.066(1)	0.61(2)
7.5	3.2(5)	0.094(1)	0.69(2)
2	10.5(6)	0.130(3)	0.79(3)

by T_0, suggests both behaviours result from the same underlying phase. We note that this change on T_0 occurs over a temperature range that is small when compared with both the magnitude of the Weiss temperature and the temperature range of the super-paramagnetic region.

5. Discussion

Bulk magnetic responses similar to $NH_4Ni_2Mo_2O_{10}H_3$ have been seen in several $S = 1$ kagome magnets (table 3): $[C_6N_2H_8][NH_4]_2[Ni_3F_6(SO_4)_2]$ [35], $(NH_4)_2(C_2H_8N)[V_3F_{12}]$ [36] and $NH_4Ni_{2.5}V_2O_7(OH)_2 \cdot H_2O$ [37]. Each of these materials displays a small ferromagnetic hysteresis in isothermal $M(H)$ data despite antiferromagnetic Weiss temperatures. While in both $[C_6N_2H_8][NH_4]_2[Ni_3F_6(SO_4)_2]$ and $(NH_4)_2(C_2H_8N)[V_3F_{12}]$ the occupation of the moment-bearing position is nominally 100 %, both $NH_4Ni_2Mo_2O_{10}H_3$ and $NH_4Ni_{2.5}V_2O_7(OH)_2 \cdot H_2O$ have occupancy factors that are significantly depleted, 64 % and 77 %, respectively. The Weiss mean-field of $NH_4Ni_2Mo_2O_{10}H_3$ is stronger than $NH_4Ni_{2.5}V_2O_7(OH)_2 \cdot H_2O$ despite the greater magnetic site occupancy of $NH_4Ni_{2.5}V_2O_7(OH)_2 \cdot H_2O$ and limited difference in their Ni–O(H)–Ni exchange pathways. The contrast in the Weiss field strength is likely to result from

Table 3. Key properties relating to magnetism for $S = 1$ KAFM systems $NH_4Ni_2Mo_2O_{10}H_3$ (present work), $NH_4Ni_{2.5}V_2O_7(OH)_2 \cdot H_2O$ [37], $[C_6N_2H_8][NH_4]_2[Ni_3F_6(SO_4)_2]$ [35] and $(NH_4)_2(C_2H_8N)[V_3F_{12}]$ [36] which display antiferromagnetic mean fields and ferromagnetic hysteresis.

	θ_W (K)	T_C (K)	Superexchange angles (°)
$NH_4Ni_2Mo_2O_{10}H_3$	−73	13.5	98.66 (12) / 85.71 (19)
$NH_4Ni_{2.5}V_2O_7(OH)_2 \cdot H_2O$	−42	17	103.33 (7) / 87.32 (10)
$[C_6N_2H_8][NH_4]_2[Ni_3F_6(SO_4)_2]$	−60	∼13	129.82 (17)
$(NH_4)_2(C_2H_8N)[V_3F_{12}]$	−30	15	149.02 / 156.95

the contribution of other exchange parameters, for example, superexchange facilitated by the Mo^{6+} and V^{5+} diamagnetic cations, such as observed for the KAFM volborthite ($Cu_3V_2O_7(OH)_2 \cdot 2\,H_2O$) which has dominant Cu–O–V–O–Cu nearest-neighbour superexchange [63].

Although the different magnitude of interactions in $NH_4Ni_{2.5}V_2O_7(OH)_2 \cdot H_2O$ and $NH_4Ni_2Mo_2O_{10}H_3$ mean direct comparison between the strength of T_0 and f cannot be drawn, the similar trends in the extracted T_0 and f components with temperature, alongside the significant site depletion of their kagome lattices, suggests related ground states. The non-magnetic site quenched disorder is commonly seen as a key requirement for spin glass-like states, but it is also possible that frustration inherent to the antiferromagnetic kagome lattice is able to stabilise a ferromagnetic component from being destroyed by site-disorder through the formation of 'canted local states' (CLS) around the spin-defects. Villain stated the combination of frustration and a sufficient number of non-magnetic impurities can always create a CLS, and further showed CLS formation can enhance the length over which ferromagnetic interactions act, via an effective dipolar interaction in his original work [64]. Such canted states would be similar to the paramagnet-like 'orphan spin states' seen in other frustrated magnets, such as SCGO(x) [65] and could so give rise to the Brillouin-like response also seen in these materials. The local exchange field of the CLS are expected to produce order known as a 'semi spin glass' state which is a combination of z ferromagnetic component and transverse spin glass order. The $\chi'(T)$ frequency dependence, split peak response in $\chi''(T)$, and ferromagnetic signal suggests such a semi spin glass state in $NH_4Ni_2Mo_2O_{10}H_3$.

Following the assumption that the ferromagnetic components seen in the aforementioned $S = 1$ kagome magnets are directed by the in-plane Dzyaloshinsky–Moriya [66, 67] (D–M) vectors to be perpendicular to the kagome lattice [68], we then propose that the ferromagnetic ordering in $NH_4Ni_2Mo_2O_{10}H_3$ is perpendicular to the kagome plane and are stabilised by transverse canting in an antiferromagnetic kagome spin texture around quenched site-disorder. Such a juxtaposition structure would be sensitive to anisotropic energy terms such as antisymmetric D–M exchange and spin-anisotropy, and also the nature of the ground state from which the CLS are developed. The role of the $S = 1$ nature of Ni^{2+} is unclear, but we speculate that it may support this juxtaposition of behaviours.

6. Conclusion

A preliminary study of $NH_4Ni_2Mo_2O_{10}H_3$ as a model $S = 1$ kagome magnet is presented. Despite occupation of the kagome site being at ≈64%, magnetometry data show common characteristics of magnetic frustration, namely the suppression of magnetic order below $|\theta_W|$ and an extended temperature range (25–225) K over which superparamagnetic correlations develop. Below ∼10 K bifurcation of field-cooled and zero-field cooled data, and coercivity in the isothermal field-dependence indicate the presence of a weak ordered ferromagnetic component. These results alongside frequency-dependent shifts in the ac-susceptibility maximum and the dc-field dependent changes to the peak suggest semi spin glass behaviour. A Brillouin-type function is observed in this ferromagnetically ordered phase which we propose is related to canted local states around the spin defects.

ORCID iDs

E T Connolly https://orcid.org/0000-0001-6103-3226
D Boldrin https://orcid.org/0000-0003-3833-8341

References

[1] Balents L 2010 *Nature* **464** 199
[2] Broholm C, Cava R J, Kivelson A, Nocera D G, Norman M R and Senthil T 2020 *Science* **367** 263

[3] Yan S, Huse D A and White S R 2011 *Science* **332** 1173
[4] Lu Y M, Ran Y and Lee P A 2011 *Phys. Rev. B* **83** 224413
[5] Iqbal Y, Becca F and Poilblanc D 2011 *Phys. Rev. B* **84** 020407(R)
[6] Li P H, Bishop R F, Campbell C E, Farnell D J, Götze O and Richter J 2012 *Phys. Rev. B* **86** 214403
[7] Messio L, Bernu B and Lhuillier C 2012 *Phys. Rev. Lett.* **108** 207204
[8] Rousochatzakis I, Wan Y, Tchernyshyov O and Mila F 2014 *Phys. Rev. B* **90** 100406
[9] Suttner R, Platt C, Reuther J and Thomale R 2014 *Phys. Rev. B* **89** 10980121
[10] Kolley F, Depenbrock S, McCulloch I P, Schollwöck U and Alba V 2015 *Phys. Rev. B* **91** 104418
[11] Mei J W, Chen J Y, He H and Wen X G 2017 *Phys. Rev. B* **95** 235107
[12] Shores M P, Nytko E A, Bartlett B M and Nocera D G 2005 *J. Am. Chem. Soc.* **127** 13462
[13] Han T H, Helton J S, Chu S, Nocera D G, Rodriguez-Rivera J A, Broholm C and Lee Y S 2012 *Nature* **492** 406
[14] Colman R H, Ritter C and Wills A S 2008 *Chem. Mater.* **20** 2005
[15] Fåk B *et al* 2012 *Phys. Rev. Lett.* **109** 037208
[16] Götze O, Farnell D J J, Bishop R F, Li P H Y and Richter J 2011 *Phys. Rev. B* **84** 224428
[17] Farnell D J, Götze O, Schulenburg J, Zinke R, Bishop R F and Li P H 2018 *Phys. Rev. B* **98** 224402
[18] Pati S K and Rao C N R 2005 *J. Chem. Phys.* **123** 234703
[19] Nishimoto S and Nakamura M 2015 *Phys. Rev. B* **92** 140412
[20] Ixert D, Tischler T and Schmidt K P 2015 *Phys. Rev. B* **92** 174422
[21] Changlani H J and Läuchli A M 2015 *Phys. Rev. B* **91** 100407
[22] Ghosh P, Verma A K and Kumar B 2016 *Phys. Rev. B* **93** 14427
[23] Hida K 2000 *J. Phys. Soc. Japan* **69** 4003
[24] Damle K and Senthil T 2006 *Phys. Rev. Lett.* **97** 067202
[25] Xu C and Moore J E 2007 *Phys. Rev. B* **76** 104427
[26] Wada N, Kobayashi T, Yano H, Okuno T, Yamaguchi A and Awaga K 1997 *J. Phys. Soc. Japan* **66** 961
[27] Kato H, Kato M, Yoshimura K and Kosuge K 2001 *J. Phys. Soc. Japan* **70** 1404
[28] Awaga K, Okuno T, Yamaguchi A, Hasegawa M, Inabe T, Maruyama Y and Wada N 1994 *Phys. Rev. B* **49** 3975
[29] Kato H, Kato M, Yoshimura K and Kosuge K 2001 *J. Phys.: Condens. Matter* **13** 9311
[30] Hara S, Sato H and Narumi Y 2012 *J. Phys. Soc. Japan* **81** 073707
[31] Kato M, Hori T, Oba N, Yoshimura K and Goto T 2003 *Physica B* **329** 1042
[32] Freedman L, Zon R, McQueen T M, Lee Y S, Payen C and Nocera D G 2012 *Chem. Commun.* **48** 64
[33] Li B, Wan Z, Song Y, Ma Z, Zhao Y, Wang J and Li Y 2023 *J. Phys.: Condens. Matter* **35** 505801
[34] Miiller W, Christensen M, Khan A, Sharma N, Macquart B, Avdeev M, Mcintyre G J, Piltz R O and Ling C D 2011 *Chem. Mater.* **3** 1315
[35] Behera J N and Rao C N R 2006 *J. Am. Chem. Soc.* **128** 9334
[36] Aidoudi F H, Downie L J, Morris R E, De Vries M A and Lightfoot P 2014 *Dalton Trans.* **43** 6304
[37] Connolly E T, Reeves P, Boldrin D and Wills A S 2018 *J. Phys.: Condens. Matter* **30** 025801
[38] Levin D, Soled S L and Ying J Y 1996 *Inorg. Chem.* **35** 4191
[39] Wu C D, Lu C Z, Lin X, Lu S F, Zhuang H H and Huang J S 2004 *J. Alloys Compd.* **368** 342
[40] Mitchell S, Gómez-Avilés A, Gardner C and Jones W 2010 *J. Solid State Chem.* **183** 198
[41] Liu H, Yin C, Liu B, Li X, Li Y, Chai Y and Liu C 2014 *Energy Fuels* **28** 2429
[42] Liu H, Yin C, Zhang H and Liu C 2016 *Chin. J. Catal.* **37** 1502
[43] Bain G A and Berry J F 2008 *J. Chem. Educ.* **85** 532
[44] Feng X, Deng Y and Blöte H W J 2008 *Phys. Rev. E* **78** 031136
[45] Henley C L 2001 *Can. J. Phys.* **79** 1307
[46] Kawamura H and Uematsu K 2019 *J. Phys.: Condens. Matter* **31** 504003
[47] Li Y, Pan B, Li S, Tong W, Ling L, Yang Z, Wang J, Chen Z, Wu Z and Zhang Q 2014 *New J. Phys.* **16** 093011
[48] Gomilšek M, Klanjšek M, Pregelj M, Luetkens H, Li Y, Zhang Q M and Zorko A 2016 *Phys. Rev. B* **94** 024438
[49] Goodenough J B 1955 *Phys. Rev.* **100** 564
[50] Kanamori J 1959 *J. Phys. Chem. Solids* **10** 87
[51] Nanda K K, Thompson L K, Bridson J N and Nag K 1994 *J. Chem. Soc. Chem. Commun.* **11** 1337
[52] Paine T K, Rentschler E, Weyhermüller T and Chaudhuri P 2003 *Eur. J. Inorg. Chem.* **2003** 3167
[53] Das A, Klinke F J, Demeshko S, Meyer S, Dechert S and Meyer F 2012 *Inorg. Chem.* **51** 8141
[54] Connolly E T 2019 *PhD Thesis* University College London
[55] Hiroi Z, Yoshida H, Okamoto Y and Takigawa M 2009 *J. Phys. Conf. Ser.* **145** 012002
[56] Colman R, Sinclair A and Wills A S 2010 *Chem. Mater.* **22** 5774
[57] Mulder C A M, van Duyneveldt A J and Mydosh J A 1981 *Phys. Rev. B* **23** 1384
[58] Mydosh J A 1993 *Spin Glasses: An Experiment Introduction* (Taylor and Francis)
[59] Thota S and Seehra M S 2013 *J. Appl. Phys.* **113** 203905
[60] Douglas N, Nakashima S and Scott J F 1984 *Phys. Rev. B* **29** 5602
[61] Han T H, Singleton J and Schlueter J A 2014 *Phys. Rev. Lett.* **113** 227203
[62] Bert F, Nakamae S, Ladieu F, Hôte D L, Bonville P, Duc F, Trombe J and Mendels P 2007 *Phys. Rev. B* **76** 132411
[63] Janson O, Furukawa S, Momoi T, Sindzingre P, Richter J and Held K C 2016 *Phys. Rev. Lett.* **117** 037206
[64] Villain J 1974 *Z. Phys.* **33** 31
[65] Schiffer P and Daruka I 1997 *Phys. Rev. B* **56** 13712
[66] Dzyaloshinsky I E 1958 *J. Phys. Chem. Solids* **4** 241
[67] Moriya T 1960 *Phys. Rev.* **120** 91
[68] Elhajal M, Canals B and Lacroix C 2002 *Phys. Rev. B* **66** 014422